Published in final edited form as:
*Biomaterials*. 2014 April ; 35(13): 4026–4034. doi:10.1016/j.biomaterials.2014.01.064.

# 3D Printing of Composite Calcium Phosphate and Collagen Scaffolds for Bone Regeneration

**Jason A. Inzana**[a,b], **Diana Olvera**[a,b], **Seth M. Fuller**[d], **James P. Kelly**[d,e], **Olivia A. Graeve**[d,e], **Edward M. Schwarz**[a,b,c], **Stephen L. Kates**[a,b,c], and **Hani A. Awad**[a,b,c,#]

[a]Center for Musculoskeletal Research, University of Rochester Medical Center, 601 Elmwood Avenue, Box 665, Rochester, NY 14642, United States

[b]Department of Biomedical Engineering, University of Rochester, 207 Robert B. Goergen Hall, Rochester, NY 14642, United States

[c]Department of Orthopaedics, University of Rochester Medical Center, 601 Elmwood Avenue, Rochester, NY 14642, United States

[d]Kazuo Inamori School of Engineering, Alfred University, 1 Saxon Drive, Alfred, NY 14802, United States

[e]Department of Mechanical and Aerospace Engineering, University of California, San Diego, 9500 Gilman Drive - MC 0411, La Jolla, CA 92093-0411, United States

## Abstract

Low temperature 3D printing of calcium phosphate scaffolds holds great promise for fabricating synthetic bone graft substitutes with enhanced performance over traditional techniques. Many design parameters, such as the binder solution properties, have yet to be optimized to ensure maximal biocompatibility and osteoconductivity with sufficient mechanical properties. This study tailored the phosphoric acid-based binder solution concentration to 8.75 wt% to maximize cytocompatibility and mechanical strength, with a supplementation of Tween 80 to improve printing. To further enhance the formulation, collagen was dissolved into the binder solution to fabricate collagen-calcium phosphate composites. Reducing the viscosity and surface tension through a physiologic heat treatment and Tween 80, respectively, enabled reliable thermal inkjet printing of the collagen solutions. Supplementing the binder solution with 1–2 wt% collagen significantly improved maximum flexural strength and cell viability. To assess the bone healing performance, we implanted 3D printed scaffolds into a critically sized murine femoral defect for 9 weeks. The implants were confirmed to be osteoconductive, with new bone growth incorporating the degrading scaffold materials. In conclusion, this study demonstrates optimization of material parameters for 3D printed calcium phosphate scaffolds and enhancement of material properties by volumetric collagen incorporation via inkjet printing.

[#]Corresponding Author. Hani A. Awad, Ph.D., University of Rochester Medical Center, 601 Elmwood Avenue, Box 665, Rochester, NY 14642, United States, Phone: 1-585-273-5268, Fax: 1-585-276-2177, hani_awad@urmc.rochester.edu.

**Disclosure**

The authors have no conflicts of interest and nothing to disclose.

## 1. Introduction

Major bone reconstruction procedures often use autografts or allografts to improve bone healing in a critically sized defect or non-union; however, these bone grafts suffer from multiple limitations that make synthetic alternatives an attractive option [1, 2]. Calcium phosphates are a primary focus for synthetic bone graft substitutes because they are osteoconductive and provide sufficient mechanical strength. Inkjet-based 3D printing has been employed to fabricate calcium phosphate scaffolds (CPS), where the calcium phosphate powder is temporarily bound by an adhesive polymer and then permanently bound by sintering of the printed green body [3, 4]. This technique, however, requires high temperatures that preclude the incorporation of bioactive molecules and drugs during the 3D printing process that could stimulate bone regeneration or combat infection.

The feasibility of low temperature 3D printing of CPS has also been demonstrated, where calcium phosphate powder is bound by aqueous (often acidic) binder solutions delivered from the inkjets through a dissolution-precipitation reaction [5–7]. In addition to enabling drug incorporation [8], low temperature 3D printing provides the potential to create composites with synthetic or biological polymers such as collagen. Type I collagen is the most abundant structural protein in the human body and is a critical component of bone extracellular matrix, where it plays important roles in this mineralized tissue's strength and toughness. It has been shown that incorporating collagen into mineralized bone cements could enhance their biomechanical properties, as well as their osteoconductive and osteoinductive characteristics. For example, collagen incorporation into hand-mixed calcium phosphate cements has been shown to improve cellular attachment, viability, proliferation, and activity as well as mechanical properties [9–12]; but the feasibility of 3D printed collagen-calcium phosphate (col-CaP) composites has not been demonstrated to our knowledge. Advantages of 3D printing over molding or paste injection include patient specific geometries [13] and controlled spatial patterning of drugs or polymers within the scaffold [8]. Furthermore, few studies have assessed the in vivo performance of low temperature 3D printed CPS, and these studies have focused on ectopic models of intramuscular implantation in rats [6, 14] and goats [15] and orthotopic models of cranial healing in rabbits [16] and dogs [5]. While these models demonstrated promising results, long bone healing might be more challenging based on differences in matrix composition and in vivo loading [17], and differences between osteochondral and intramebraneous bone formation processes that contribute differently to the healing of long and cranial bones, respectively [18, 19].

To address these points, this study focused first on optimizing the formulation of the acidic binder solution used in low temperature 3D printing of CPS for optimized accuracy, mechanical strength, and biocompatibility. Next, we evaluated the in vivo regenerative potential of these 3D printed CPS in a critically sized murine femoral defect. We hypothesized that col-CaP composites could be fabricated through low temperature 3D printing by dissolving collagen into the phosphoric acid binder solution; and that these composites will improve the scaffold's mechanical strength, cytocompatibility and bone regeneration in a critically sized femoral defect.

## 2. Materials and Methods

### 2.1 Powder and binder solution formulations

Dilutions of phosphoric acid (5–20 wt%) were used as the base binder solution for 3D printing the CPS. Tween 80 (Sigma-Aldrich, St. Louis, MO), a non-cytotoxic surfactant, was added to some of the binder formulations at a concentration of 0.25 wt% based on the approximate critical micelle concentration in phosphate buffer [20].

Lyophilized bovine dermal type I collagen was kindly provided by Kensey Nash (Exton, PA). Collagen solutions were prepared by dissolving the collagen into phosphoric acid at 4°C until completely dissolved and then stored at 4°C until use. Concentrations of each solution were confirmed by optical absorbance at 280 nm and compared with a linear standard curve using a spectrophotometer (Synergy Mx Microplate Reader, BioTek Instruments Inc.; Winooski, VT).

The calcium phosphate powder was prepared by solution combustion synthesis following similar procedures as described previously [21–23]. As an initial step, a mixture of 12.1058 g of $Ca(NO_3)_3{\bullet}4H_2O$ (Alfa Aesar #A16645), 3.9433 $(NH_4)_2HPO_4$ (Alfa Aesar #11597), and 6.9270 g of carbohydrazide (Alfa Aesar #A11145) was mixed in a Pyrex crystallization dish with water as the solvent. The mixture was then placed in a muffle furnace at 500°C and allowed to combust, taking approximately 15 minutes for the reaction to complete. After synthesis, the powders were crushed in a mortar and pestle and subsequently calcined at 1300°C for 2 hours. The resulting powder was a composite of hydroxyapatite and α-tricalcium phosphate (Fig. S1).

### 2.2 Adaptation of a commercial 3D printer and preparation of 3D printed scaffolds

A ZPrinter® 450 (3D Systems; Andover, MA) was adapted to print with calcium phosphate powder and acidic binder solutions using bench scale volumes (≥50 g of powder). The binder solution fluid lines were replaced with polypropylene or polytetrafluoroethylene (PTFE) tubing and an inert glass reservoir was added to avoid degradation by the acidic solutions. A custom overhead powder distribution system and build chamber (60 × 60 × 30 mm) were employed to isolate the biomaterials during the 3D printing process and allow formation of a packed powder bed in a smaller area (Fig. S2). The new powder feed system was linked via a belt mechanism to the motor of the original equipment manufacturer's (OEM) powder feed system to exploit the automated software control of the 3D printing process. For all experiments, the powder layer thickness was set to 89 μm and the binder liquid/powder ratio was set as 0.46 (homogenous) in the ZPrint™ software. The phosphoric acid-based binder solutions were delivered by thermal inkjets (HP11, Hewlett-Packard; Palo Alto, CA) to selectively bind the powder, which produces dicalcium phosphate dihydrate (DCPD or brushite; Fig. S1). After printing, the samples were post-processed by flash dipping in 0.1 wt% phosphoric acid and then washing in deionized water (3×120 seconds) to improve surface binding and remove residual acidity. Some samples were coated with collagen by dipping them into a 0.5 wt% collagen in 0.1 wt% phosphoric acid solution, neutralized to pH 7 with NaOH, and allowing to air dry. For in vivo experiments, the scaffolds were sterilized by supercritical $CO_2$ (NovaSterilis, Lansing, NY).

### 2.3 Characterization of binder solutions and printability

Considering that fluid properties dictate the printability of a solution via inkjets, the density, viscosity, surface tension, and printing saturation of the binder solutions were measured. The viscosities were measured using a 40 mm cone-plate rheometer (Discovery HR-2, TA Instruments; New Castle, DE) at 25°C and a shear rate of 100 $s^{-1}$, except for shear rate-dependent experiments where data was collected from 25–630 $s^{-1}$. The fluid surface tensions were measured on a Model 500 Goniometer (Ramé-Hart Instrument Co., Succasunna, NJ) at 20°C and were averaged over at least 40 points on multiple droplets. Printing saturation was quantified by measuring the mass of binder fluid printed into weighing boats, converting to volume, and normalizing to the theoretical powder volume. Four measurements were made per print job, averaging over 5 layers for each measurement, with 2 different ink cartridges per binder formulation. To investigate the accuracy of the HP 11 print heads over a range of viscosities, a series of 1 mm lines were printed onto blue litmus paper to visualize the acidic solutions. The accuracy was quantified with a custom MATLAB algorithm (R2013a; MathWorks Inc.; Natick, MA) by overlaying the ideal line set atop the image of the printed lines and calculating the area of erroneous printing (Fig. S3*a*,*b*).

### 2.4 Optimization of calcium phosphate powder particle size

The powder particle size distribution is critical for enabling a well-packed, smooth powder bed for printing and also for dictating the intrinsic micro-porosity and resolution of the printed material [7]. Therefore, the calcium phosphate powder was sieved and collected from between two stainless steel meshes (ranging 30–150 μm) to remove particulate that was too large for accurate printing and too small to avoid agglomeration. Solid elliptical cylinders that represent the outer dimensions of a mouse femoral diaphysis (1.2 × 2 × 3 mm) were printed with each particle size range and imaged by high-resolution micro-computed tomography (micro-CT; VivaCT 40, Scanco Medical; Bassersdorf, Switzerland) with a 10.5 μm isotropic voxel size using an integration time of 300 ms, energy of 55 kV, and intensity of 145 μA. Three-dimensional renderings of the micro-CT images were co-registered with the computer-aided design (CAD) image that was used to guide the printing process and the error was quantified by volumetric differences between the overlaid images (Fig. 2*a*). 3D image reconstruction and quantitative analysis was performed using Amira software (Amira 5.4.5, FEI Visualization Sciences Group; Burlington, MA).

### 2.5 Material characterization of 3D printed scaffolds

The flexural properties of the 3D printed CPS were assessed by 3 point bending since cements tend to be most susceptible to shear and tensile failure. Samples were 3D printed as 4 × 1 × 14 mm bars and tested on a 10 mm support span using an Instron 8841 DynaMight™ Axial Testing System (Instron Corp.; Canton, MA) with a 50 N load cell. Flexural tests were performed at a displacement rate of 1 mm/min until failure.

The volumetric porosity and pore size distributions were estimated from micro-CT images using Amira. The pore size distributions were measured using Amira's surface thickness algorithm, which calculates the distance of the normal projection from each facet on the triangulated surface to the intersection with the next surface.

Scanning electron microscopy (SEM; LEO 982 FE-SEM, Carl Zeiss SMT; Thornwood, NY) of gold-sputtered samples was used for qualitative assessment of the scaffold surfaces and porosity. X-ray diffraction (XRD; X'Pert PRO MRD; PANalytical, Westborough, MA) spectra were acquired to qualitatively assess phase composition of the calcium phosphate powder and 3D printed samples. Spectra were acquired from $2\theta = 20–40°$ with a step size of 0.02°.

### 2.6 In vitro cytocompatibility of 3D printed CPS materials

**2.6.1 Cytotoxicity analysis based on ISO 10993 for preliminary screening—**The cytocompatibility of the scaffold materials was assessed by XTT assay with C3H/10T1/2 cells (ATCC; Manassas, VA) exposed to media extracts as described by ISO 10993-5. Extraction was performed according to the mass-based ratios of ISO 10993-12 in sealed tubes within a static incubator at 37°C and 95% humidity for 24 hours. PTFE and PVC were used as negative and positive controls for toxicity, respectively. Viability measurements were normalized to media-only controls.

**2.6.2 Viability of cells cultured on 3D printed CPS materials—**Samples were 3D printed as 1.2 mm thick discs with a 6.3 mm diameter to completely cover the well bottoms in a 96 well plate. C3H/10T1/2 cells were seeded onto the discs in the wells at 10,000 cells/well. After 24 or 72 hours, the cell viability was measured by a live-dead fluorescence assay (MultiTox-Fluor Cytotoxicity Assay, Promega Corp.; Madison, WI). The relative cell viability is reported as the ratio of live signal intensity to dead signal intensity, after subtracting intensities of acellular controls and normalizing to cells on tissue culture plastic.

### 2.7 In vivo evaluation of bone healing in a critically sized murine femoral defect

**2.7.1 Animals and surgical procedures—**All animal studies were performed in accordance with protocols approved by the University of Rochester's Committee on Animal Resources. Female BALB/cJ mice were purchased from Jackson Research Labs (Bar Harbor, ME) at 13–15 weeks of age and acclimated for one week prior to surgery. The right femur was exposed by a direct lateral approach and a radiolucent polyether ether ketone (PEEK) plate with a 40 nm titanium coating was installed across the anterolateral surface using 4 titanium screws (RISystem; Davos, Switzerland). A 2 mm osteotomy was created at the femoral mid-shaft using a 0.22 mm wire gigli saw and a cutting guide to ensure reproducible size and placement [24]. A devitalized allograft or a 3D printed scaffold was placed into the 2 mm defect and secured to the plate with a 5-0 nylon suture or the defect was left empty (n=4/group). Devitalized allografts were prepared from 15-week-old female C57Bl/6J mice as previously described [25]. The wound was closed and allowed to heal for 9 weeks, at which point the mice were euthanized for tissue harvest and analysis.

**2.7.2 Radiographic imaging and quantification—**To monitor the progress of bone healing, X-rays (LX-60 X-ray Cabinet, Faxitron Bioptics LLC; Tucson, AZ) were taken weekly at an exposure of 5 s and energy of 26 kV. After 9 weeks of healing, the femurs were scanned ex vivo by micro-CT at a 10.5 μm isotropic resolution using an integration time of 300 ms, energy of 55 kV, and intensity of 145 μA. The mineralized volume, mineral density and mineral content were measured from a 2 mm region (190 slices) corresponding with the

initial defect. Average volumes of representative scaffolds and allografts were subtracted from the mineralized volumes to yield the net mineralized volume, which measures changes due to new bone formation as well as scaffold resorption. The volume of new bone that contained scaffold particulate (engraftment volume) was quantified by manual contouring coupled with automated edge detection in the 2D micro-CT slices (Fig. 6*c*).

**2.7.3 Biomechanical properties of healing defects—**The torsional properties of each femur were measured, as described previously [26], to assess the functional progress of the healing defects. Briefly, the ends of the femur were embedded in poly(methyl methacrylate) bone cement (DePuy; Warsaw, IN) within square aluminum tubes and then rehydrated in phosphate buffered saline for 2 hours. Prior to testing, the specimen was mounted in the grips and the fixation plate and screws were removed. The specimens were tested in torsion at a rate of 1 deg/s up to 40 degrees of rotation or failure using an EnduraTec TestBench™ (Bose Corp.; Minnetonka, MN) with a 200 N-mm torque cell.

### 2.8 Data Analysis

Results were analyzed by analysis of variance (ANOVA) with appropriate corrections for multiple comparisons as indicated within each results section or figure. Data from each metric were confirmed to satisfy assumptions of a Gaussian distribution based on the D'Agostino-Pearson normality test or a non-parametric alternative was used where appropriate. Differences were considered significant for $p < 0.05$.

## 3. Results

### 3.1 Optimization of phosphoric acid-based binder solutions

Formulation of optimal binder solutions for 3D printing calcium phosphates must consider biocompatibility as well as material strength. Higher binder solution acidities will produce scaffolds with greater strength [6], but higher acidities will also result in greater cytotoxicity. Using 12.5 wt% phosphoric acid results in nearly complete cell death (15.7% ± 0.8% viability) due to residual acid that caused the media pH to drop below 5. Reducing the acid concentration to 8.75 wt% significantly improves cell viability (59.4% ± 3.8% viability); and no further improvements were observed by reduction to 5 wt% (68% ± 6.0% viability; Fig. 1*a*). Using 8.75 wt% phosphoric acid produces significantly stronger scaffold materials over 5 wt% (Fig. 1*b*). Therefore, 8.75 wt% phosphoric acid was selected for all subsequent experiments.

The printing accuracy of the HP11 inkjets was found to be anisotropic with minimal error below 3 mPa-s (Fig. S3*c*). The anisotropic resolution is important for designing the orientation of small pores within the build chamber, such as those used for the intramedullary canal of mouse scaffolds (Fig. 3*a*). In addition to limiting the viscosity, supplementing the binder formulations with 0.25 wt% Tween 80 improves printing saturations by reducing the solution's surface tension (Table 1). The improved printing with Tween 80 significantly increases the strength of the 3D printed CPCs, without compromising the cytocompatibility (Fig. 1).

### 3.2 Optimization of printing accuracy based on powder particle size

Using powder collected from between a 30 μm mesh and a 50 μm or 70 μm mesh produced mouse-sized scaffolds with minimal error relative to the original CAD drawing (Fig. 2*b*). The scaffold's porosity and pore size distributions did not differ significantly between a 50 μm and 70 μm mesh as the upper limit (Fig. 2*c*,*d*), so powder for future experiments was collected from between 30 μm and 70 μm sieves for maximum material yield.

SEM images of a mouse-sized scaffold, modeled after the femoral mid-diaphysis, demonstrate successful printing of an open intramedullary canal that may be important for bone ingrowth and reestablishing the marrow compartment (Fig. 3*a*). Examining the micro-porosity of the 3D printed scaffolds confirms pore sizes in the range of 20–50 μm (Fig. 3*b*), which is consistent with the micro-CT measurements (Fig. 2*d*). Plate-like crystal growth on the surfaces of unreacted powder particulate (Fig. 3*d*) may be important for increasing the specific surface area for protein or drug adsorption.

### 3.3 Collagen solutions as the binding agent for 3D printed CPS

**3.3.1 Characterization of phosphoric acid-based collagen solutions for inkjet printing—**Collagen solution viscosity was found to vary dramatically with the concentrations of collagen and phosphoric acid (Fig. 4*a*). At 5 and 8.75 wt% acid, the viscosity increases exponentially with collagen concentration to levels that are not printable from these inkjets (>5 mPa-s). When the acid concentration is at least 12.5 wt%, however, only small variations in viscosity are observed with increasing collagen concentrations. Considering that 8.75 wt% acid was found to be a good balance between cytocompatibility and material strength (Fig. 3), collagen solutions using this acid concentration were warmed to 37°C for 30 minutes to produce fluids with printable viscosities (Fig. 4*a*). Collagen naturally forms fibrillar chains and the interactions among these chains cause drag forces that produce the exponential increases in viscosity. Solutions of polymer chains generally exhibit shear thinning, which is observed in the 5 and 8.75 wt% phosphoric acid solutions containing intact collagen chains (Fig. 4*b*). The higher acidities (≥12.5 wt%) or transient heat treatment at 37°C likely cause disassembly of these chains as demonstrated by the lower viscosities and transition to Newtonian behavior (Fig. 4*a*,*b*). The HP11 cartridge uses thermal inkjet technology to rapidly heat the solution, which produces a small bubble to eject each fluid droplet. While the primary heating is focused to a minute volume in the nozzles, the rest of the printing solution can also experience increases in temperature. Therefore, the collagen chains will be denatured even if the solution is not pre-warmed to achieve the reduced viscosity (Fig. 4*c*). The solutions printed from the inkjets were confirmed to maintain at least 94% of the collagen originally in solution based on the optical absorbance at 280 nm (Fig. 4*d*). A 1.5 wt% collagen in 8.75 wt% phosphoric acid solution was used as the binder to 3D print a col-CaP composite and the presence of collagen within the cement was supported by SEM imaging (Fig. 4*e*).

While the addition of collagen to the phosphoric acid binder solutions significantly reduces the surface tension, it does not improve the printing saturation. The collagen solutions often exhibit streaking or a heterogeneous saturation, which may result from partial or transient clogging of the nozzles during the printing process. This effect is mitigated by the addition

of 0.25 wt% Tween 80 to produce equivalent printing saturations between collagen and acid binder solutions (Table 1).

**3.3.2 Functional performance of 3D printed collagen-CaP composites—**Adding collagen into the binder solution (8.75 wt% phosphoric acid + 0.25 wt% Tween 80) significantly improves the strength of the 3D printed CPS as a linear function of collagen concentration (Fig. 5*a*). Considering that the printed collagen does not form fibrillar networks, this volumetric collagen incorporation is unable to mitigate the brittleness of these materials. Alternatively, CPS that were printed without collagen in the binder solution were coated with a 0.5 wt% neutralized collagen gel that dried into a film on the surface. This collagen coating dramatically improved the maximum flexural strength as well as the toughness (Fig. 5*b*). Further, supplementing the binder solution with 1 wt% collagen significantly improves the viability of C3H/10T1/2 cells cultured on the scaffold materials for up to 72 hours. The cell viability is also increased significantly by coating the samples with 0.5 wt% neutralized collagen (Fig. 5*c*).

### 3.4 Efficacy of 3D printed CPS as bone graft substitutes in a murine femoral defect model

X-rays of the bone healing time course and micro-CT imaging at 9 weeks qualitatively demonstrate similar levels of new bone formation between allografts and 3D printed scaffolds (Fig. 6*a,b*). New bone growth tended to proceed primarily through the intramedullary canal with some periosteal bone formation, which was predominant on the distal side, in both the 3D printed scaffolds and allografts. As bone growth proceeded along the scaffolds, they tended to be partly broken down and incorporated into the newly forming bone (Fig. 6*c*). None of the scaffolds or allografts enabled host-host bridging. 3D printed CPS that were coated with a 0.5 wt% neutralized collagen tended to facilitate less new bone formation (Table 2). The specimens without a scaffold or allograft implant were unable to heal, confirming the 2 mm defect is critically sized. The mineral density, mineral content, and net mineralized volume were similar across all of the scaffold groups (Table 2). The collagen coated implants, however, tended to generate less bone ingrowth as measured by the mineral content and scaffold engraftment volume (Table 2). The allografts tended to have the greatest net mineralized volume and achieved significantly higher maximum torque values, but allografts do not dissolve or resorb as readily as the 3D printed scaffolds. None of the treatments approached the torsional strength of intact murine femurs, which achieve a maximum torque of 19.4 ± 5.6 N.mm [25].

## 4. Discussion

In this study, a commercial 3D printer was adapted to create composite bone graft substitutes for tissue engineering applications and preclinical studies of bone healing in small animal models. While other studies have investigated parameters related to the powder, such as chemical composition [27, 28] and particle size [7], the current study focused on enhancing 3D printed CPS through alternative binder solution formulations.

The primary advantages of low temperature 3D printing in biomaterials applications is the potential to create polymer-mineral composites with enhanced material properties or include drugs and growth factors to improve bone healing or combat infection [8]. However, the

acidic binder solutions commonly used with this low temperature technique can pose issues for biocompatibility. The residual acidity may be removed by thoroughly rinsing the samples [29], but this would also elute any bioactive molecules that were printed into the constructs. Considering that the incorporation of growth factors and other drugs holds great promise for applications in tissue engineering and bone regeneration, the thorough rinsing technique was avoided in this study. Greater material strengths could also be achieved by sintering the scaffolds, but the high temperatures would be counter-productive to incorporating heat-labile molecules such as proteins. Instead, an optimal balance between cytocompatibility and material strength was achieved by using 8.75 wt% phosphoric acid as the binder solution.

Further formulation of the binder solutions investigated the beneficial effects of adding a non-cytotoxic surfactant as well as type I collagen. The importance of reducing the surface tension of fluids for inkjet printing is well established; however, the effects of surfactants in phosphoric acid-based binder solutions have not yet been investigated in the context 3D printed calcium phosphates. The current study confirms the benefits of 0.25 wt% Tween 80 for improving the printability of the binder solutions, which enhanced the mechanical strength of the printed materials without compromising the biocompatibility. The addition of Tween 80 along with a physiologic heat treatment also enabled reliable inkjet printing of collagen solutions to improve the mechanical strength and cellular viability. In vivo, type I collagen assembles into fibers that make it one of the key structural proteins of the extracellular matrix. While the collagen that is printed into the composites in this study is unable to form structural fibers, the biological benefits are still evident in vitro. Hand mixing solutions of type I collagen into self-setting cements has been shown to improve cellular attachment, proliferation, and activity [9, 12], but collagen fiber formation may not occur in these materials either [9]. Collagen-mimetic short peptides, which could similarly exist in the denatured collagen used in this study, have been shown to improve bone healing when coated on the surface of biomaterial scaffolds [30]. Printing of collagen that can form fibrous networks has been demonstrated as well [31], but a dc solenoid inkjet valve with a larger diameter was employed to accommodate the viscous solution. This technique would not be useful for the powder-based 3D inkjet printing utilized in this study because of the poor resolution and disruption of the powder bed by the larger droplets.

In vivo, the 3D printed CPS enabled new bone growth into the scaffolds as they were resorbed or incorporated into the newly forming bone. The torsional strength of the allografts was significantly higher than the printed scaffolds, but the extent of new bone formation, lack of host-host bridging, and engraftment were similar. The lower strength of the scaffolds is partly attributable to the material's degradability, which enables it to be readily replaced by new bone. While the scaffolds were found to be osteoconductive, as demonstrated by engraftment of the materials into new bone, they were insufficiently osteoinductive and were unable to completely heal the defect. Similar results of osteoconduction, but incomplete healing, were evident in previous studies of 3D printed calvarial implants [5, 16]. This common result in biomaterials research has led to the theme of combinational therapies that supplement the scaffold material with growth factors and/or cells to induce new bone formation. One limitation of the in vivo study is the small sample size. However, considering that none of the treatments achieved host-host unification, the

bone defect cannot be considered as healed, regardless of the treatment, and larger sample sizes of animals were not justified for ethical considerations. Future studies that incorporate growth factors such as BMP-2 into the 3D printed scaffolds will determine if a critically sized defect can be fully healed by such synthetic bone graft substitutes.

## 5. Conclusion

This study demonstrates strategies for adapting inkjet 3D printing technology and optimization of material parameters to fabricate CPS for applications in preclinical small animal models of bone regeneration. These scaffolds are printed with high resolution to achieve versatile geometries that can include macropores as small as 0.5 mm and have microporosity that is critical for fluid exchange and cellular influx during bone healing. The materials are sufficiently strong for handling and placement into a non-loading bone defect and are degradable and osteoconductive, which allows replacement and incorporation of these scaffolds into the newly forming bone. Inkjet printing of collagen solutions with high resolution has not been previously utilized in 3D printing of calcium phosphates. This study demonstrates the feasibility of these processes and the mechanical and cellular benefits of volumetric collagen inclusion in vitro. Future in vivo studies will confirm whether the inkjet-delivered collagen improves bone healing efficacy of the 3D printed scaffolds when coupled with osteoinductive factors.

## Supplementary Material

Refer to Web version on PubMed Central for supplementary material.

## Acknowledgments

The Authors would like to thank Michael Thullen (University of Rochester) for his assistance with micro-CT, Christine Pratt (University of Rochester) for her assistance with XRD, Teresa Porri (Cornell) for her assistance in measuring the fluid surface tensions, and Gino Bradica (Kensey Nash) for the kind gift of the collagen used in these experiments. This study was supported by the AO Trauma Research Fund and NIAMS/NIH grant P30AR061307. Jason Inzana is supported by an NSF graduate research fellowship (2012116002). The content is solely the responsibility of the authors and does not necessarily represent the official views of the National Science Foundation, National Institutes of Health, or AO Foundation.

## References

1. De Long WG Jr, Einhorn TA, Koval K, McKee M, Smith W, Sanders R, et al. Bone grafts and bone graft substitutes in orthopaedic trauma surgery. A critical analysis. J Bone Joint Surg Am. 2007; 89(3):649–658. [PubMed: 17332116]
2. Kurien T, Pearson RG, Scammell BE. Bone graft substitutes currently available in orthopaedic practice: the evidence for their use. Bone Joint J. 2013; 95-B(5):583–597. [PubMed: 23632666]
3. Seitz H, Rieder W, Irsen S, Leukers B, Tille C. Three-dimensional printing of porous ceramic scaffolds for bone tissue engineering. J Biomed Mater Res B Appl Biomater. 2005; 74(2):782–788. [PubMed: 15981173]
4. Fierz FC, Beckmann F, Huser M, Irsen SH, Leukers B, Witte F, et al. The morphology of anisotropic 3D-printed hydroxyapatite scaffolds. Biomaterials. 2008; 29(28):3799–3806. [PubMed: 18606446]
5. Igawa K, Mochizuki M, Sugimori O, Shimizu K, Yamazawa K, Kawaguchi H, et al. Tailor-made tricalcium phosphate bone implant directly fabricated by a three-dimensional ink-jet printer. J Artif Organs. 2006; 9(4):234–240. [PubMed: 17171402]

6. Gbureck U, Hölzel T, Klammert U, Würzler K, Müller FA, Barralet JE. Resorbable dicalcium phosphate bone substitutes prepared by 3D powder printing. Adv Funct Mater. 2007; 17(18):3940–3945.
7. Butscher A, Bohner M, Roth C, Ernstberger A, Heuberger R, Doebelin N, et al. Printability of calcium phosphate powders for three-dimensional printing of tissue engineering scaffolds. Acta Biomater. 2012; 8(1):373–385. [PubMed: 21925623]
8. Vorndran E, Klammert U, Ewald A, Barralet JE, Gbureck U. Simultaneous immobilization of bioactives during 3D powder printing of bioceramic drug-release matrices. Adv Funct Mater. 2010; 20(10):1585–1591.
9. Tamimi F, Kumarasami B, Doillon C, Gbureck U, Le Nihouannen D, Cabarcos EL, et al. Brushite-collagen composites for bone regeneration. Acta Biomater. 2008; 4(5):1315–1321. [PubMed: 18486574]
10. Moreau JL, Weir MD, Xu HH. Self-setting collagen-calcium phosphate bone cement: mechanical and cellular properties. J Biomed Mater Res A. 2009; 91(2):605–613. [PubMed: 18985758]
11. Thein-Han W, Xu HH. Collagen-calcium phosphate cement scaffolds seeded with umbilical cord stem cells for bone tissue engineering. Tissue Eng Pt A. 2011; 17(23–24):2943–2954.
12. Perez RA, Ginebra MP. Injectable collagen/alpha-tricalcium phosphate cement: collagen-mineral phase interactions and cell response. J Mater Sci Mater Med. 2013; 24(2):381–393. [PubMed: 23104087]
13. Klammert U, Gbureck U, Vorndran E, Rodiger J, Meyer-Marcotty P, Kubler AC. 3D powder printed calcium phosphate implants for reconstruction of cranial and maxillofacial defects. J Cranio Maxill Surg. 2010; 38(8):565–570.
14. Klammert U, Ignatius A, Wolfram U, Reuther T, Gbureck U. In vivo degradation of low temperature calcium and magnesium phosphate ceramics in a heterotopic model. Acta Biomater. 2011; 7(9):3469–3475. [PubMed: 21658480]
15. Habibovic P, Gbureck U, Doillon CJ, Bassett DC, van Blitterswijk CA, Barralet JE. Osteoconduction and osteoinduction of low-temperature 3D printed bioceramic implants. Biomaterials. 2008; 29(7):944–953. [PubMed: 18055009]
16. Tamimi F, Torres J, Gbureck U, Lopez-Cabarcos E, Bassett DC, Alkhraisat MH, et al. Craniofacial vertical bone augmentation: a comparison between 3D printed monolithic monetite blocks and autologous onlay grafts in the rabbit. Biomaterials. 2009; 30(31):6318–6326. [PubMed: 19695698]
17. van den Bos T, Speijer D, Bank RA, Bromme D, Everts V. Differences in matrix composition between calvaria and long bone in mice suggest differences in biomechanical properties and resorption: Special emphasis on collagen. Bone. 2008; 43(3):459–468. [PubMed: 18583211]
18. Everts V, Korper W, Hoeben KA, Jansen ID, Bromme D, Cleutjens KB, et al. Osteoclastic bone degradation and the role of different cysteine proteinases and matrix metalloproteinases: differences between calvaria and long bone. J Bone Miner Res. 2006; 21(9):1399–1408. [PubMed: 16939398]
19. Himeno-Ando A, Izumi Y, Yamaguchi A, Iimura T. Structural differences in the osteocyte network between the calvaria and long bone revealed by three-dimensional fluorescence morphometry, possibly reflecting distinct mechano-adaptations and sensitivities. Biochem Biophys Res Commun. 2012; 417(2):765–770. [PubMed: 22198435]
20. Feng J, Zeng Y, Ma C, Cai X, Zhang Q, Tong M, et al. The surfactant tween 80 enhances biodesulfurization. Appl Environ Microbiol. 2006; 72(11):7390–7393. [PubMed: 16980422]
21. Graeve OA, Kanakala R, Madadi A, Williams BC, Glass KC. Luminescence variations in hydroxyapatites doped with Eu2+ and Eu3+ ions. Biomaterials. 2010; 31(15):4259–4267. [PubMed: 20188413]
22. Sinha K, Pearson B, Casolco SR, Garay JE, Graeve OA. Synthesis and consolidation of BaAl2Si2O8:Eu: development of an integrated process for luminescent smart ceramic materials. J Am Ceram Soc. 2009; 92(11):2504–2511.
23. Graeve OA, Varma S, Rojas-George G, Brown DR, Lopez EA. Synthesis and characterization of luminescent yttrium oxide doped with Tm and Yb. J Am Ceram Soc. 2006; 89(3):926–931.

24. Manassero M, Viateau V, Matthys R, Deschepper M, Vallefuoco R, Bensidhoum M, et al. A novel murine femoral segmental critical-sized defect model stabilized by plate osteosynthesis for bone tissue engineering purposes. Tissue Eng Pt C-Meth. 2013; 19(4):271–280.
25. Xie C, Reynolds D, Awad H, Rubery PT, Pelled G, Gazit D, et al. Structural bone allograft combined with genetically engineered mesenchymal stem cells as a novel platform for bone tissue engineering. Tissue Eng. 2007; 13(3):435–445. [PubMed: 17518596]
26. Reynolds DG, Hock C, Shaikh S, Jacobson J, Zhang X, Rubery PT, et al. Micro-computed tomography prediction of biomechanical strength in murine structural bone grafts. J Biomech. 2007; 40(14):3178–3186. [PubMed: 17524409]
27. Vorndran E, Klarner M, Klammert U, Grover LM, Patel S, Barralet JE, et al. 3D powder printing of beta-tricalcium phosphate ceramics using different strategies. Adv Eng Mater. 2008; 10(12):B67–B71.
28. Klammert U, Vorndran E, Reuther T, Muller FA, Zorn K, Gbureck U. Low temperature fabrication of magnesium phosphate cement scaffolds by 3D powder printing. J Mater Sci Mater Med. 2010; 21(11):2947–2953. [PubMed: 20740307]
29. Klammert U, Reuther T, Jahn C, Kraski B, Kubler AC, Gbureck U. Cytocompatibility of brushite and monetite cell culture scaffolds made by three-dimensional powder printing. Acta Biomater. 2009; 5(2):727–734. [PubMed: 18835228]
30. Wojtowicz AM, Shekaran A, Oest ME, Dupont KM, Templeman KL, Hutmacher DW, et al. Coating of biomaterial scaffolds with the collagen-mimetic peptide GFOGER for bone defect repair. Biomaterials. 2010; 31(9):2574–2582. [PubMed: 20056517]
31. Xu T, Binder KW, Albanna MZ, Dice D, Zhao W, Yoo JJ, et al. Hybrid printing of mechanically and biologically improved constructs for cartilage tissue engineering applications. Biofabrication. 2012; 5(1):015001. [PubMed: 23172542]

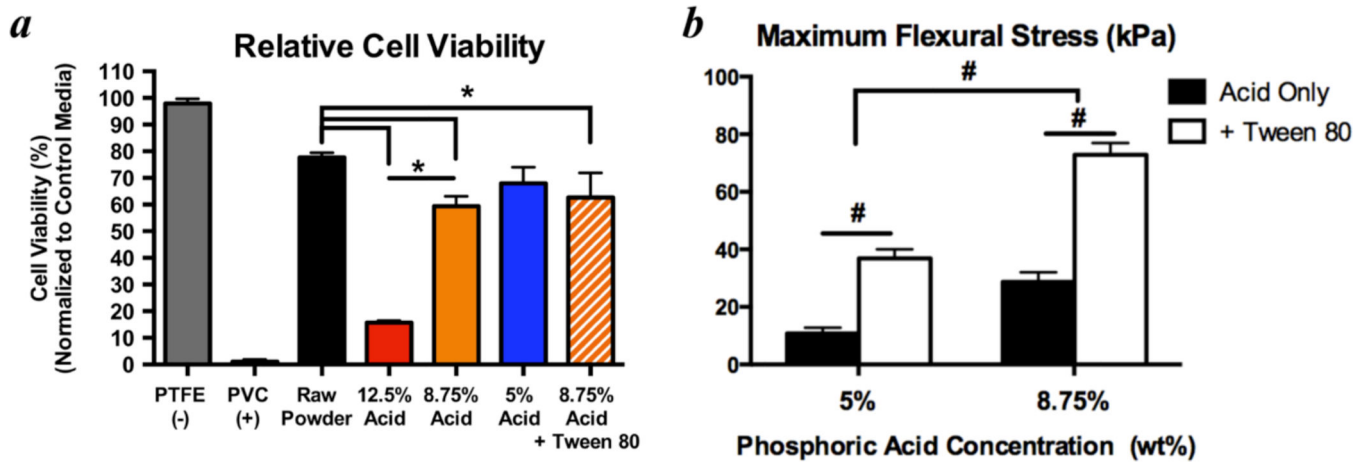


**Figure 1. Optimization of binder solution acidity to maximize cytocompatibility and mechanical strength**

*a)* Using media extraction techniques with XTT assays after 24 hours of exposure to test material cytotoxicity according to ISO 10993, significant improvements in C3H/10T1/2 cell viability were observed when decreasing binder acidity from 12.5 wt% to 8.75 wt%. No significant improvements were observed when the acidity was further decreased to 5 wt% (n=6/group). * indicates $p < 0.05$ by ANOVA with Tukey's correction for multiple comparisons. Adding a non-cytotoxic surfactant (0.25 wt% Tween 80) did not significantly change viability, however, it significantly increased the strength of the printed materials in 3 point bending (*b*) by enhancing binder solution printability into the powder. Therefore, 8.75 wt% phosphoric acid + 0.25 wt% Tween 80 was chosen as the baseline binder solution for subsequent experiments. # indicates $p < 0.05$ by 2-way ANOVA with Sidak's correction for multiple comparisons. n=6–9/group. Bars represent means and error bars are standard deviation.

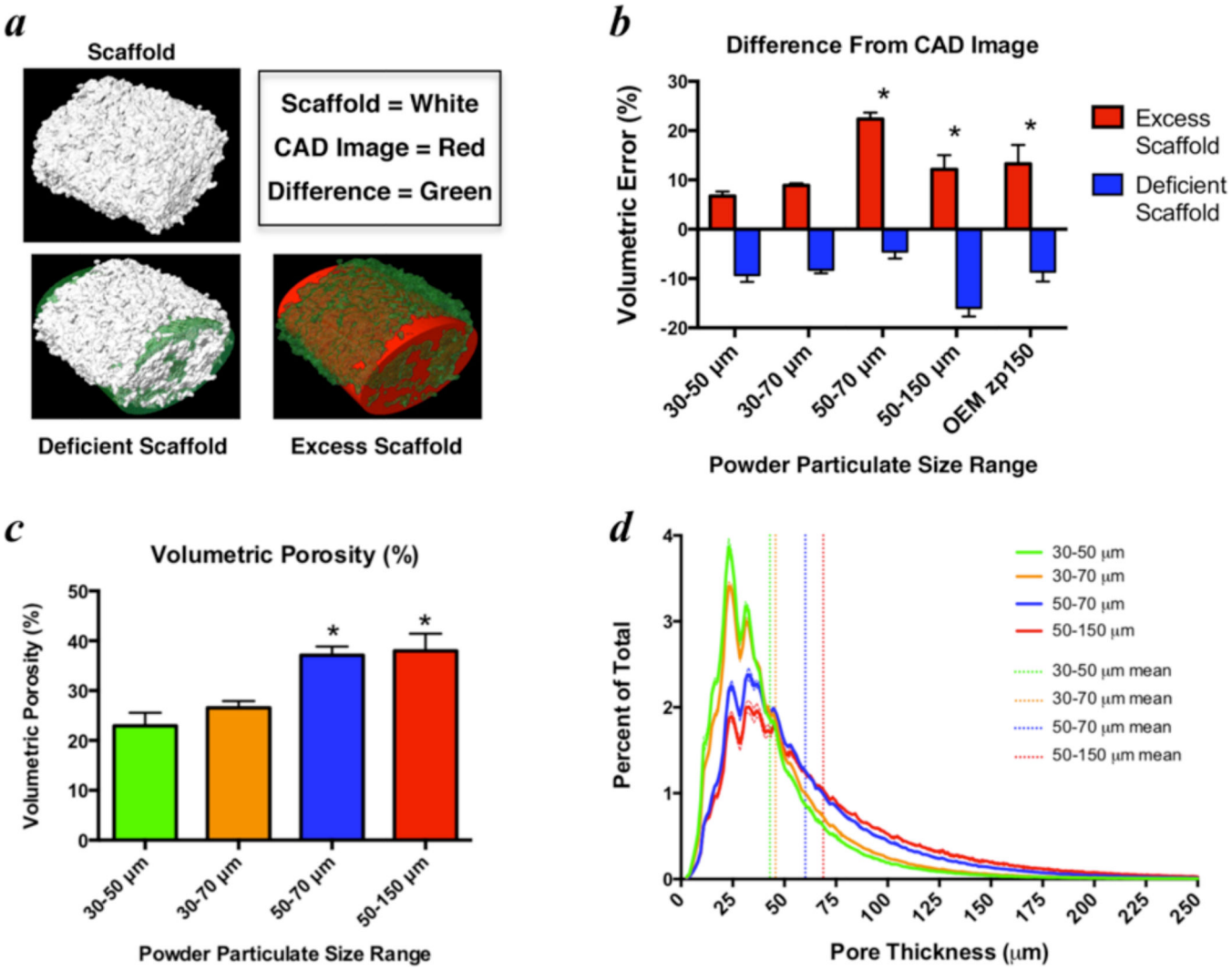


**Figure 2. Optimization of powder particle size for 3D printing accuracy of murine-sized femoral scaffolds**

*a*) 3D image renderings from micro-CT scans of 3 mm murine femoral scaffolds were used to measure the printing accuracy relative to the ideal computer-aided design (CAD) image, which was utilized to guide the printing process. *b*) Volumetric differences were quantified as the sum of deficient scaffold (where scaffold material should exist, but does not) and excess scaffold (where scaffold material exists, but should not) and were normalized to the total scaffold volume. Volumetric porosity (*c*) and pore size (*d*), estimated from the same micro-CT images, were primarily dictated by the lower limit of the powder particle size. * indicates significant differences ($p < 0.05$) from 30–50 μm powder by ANOVA with Dunnett's correction for multiple comparisons. Absolute volumetric error was used for statistical comparison in (*b*). Bars represent means and error bars are standard deviation. n=4–5/group.

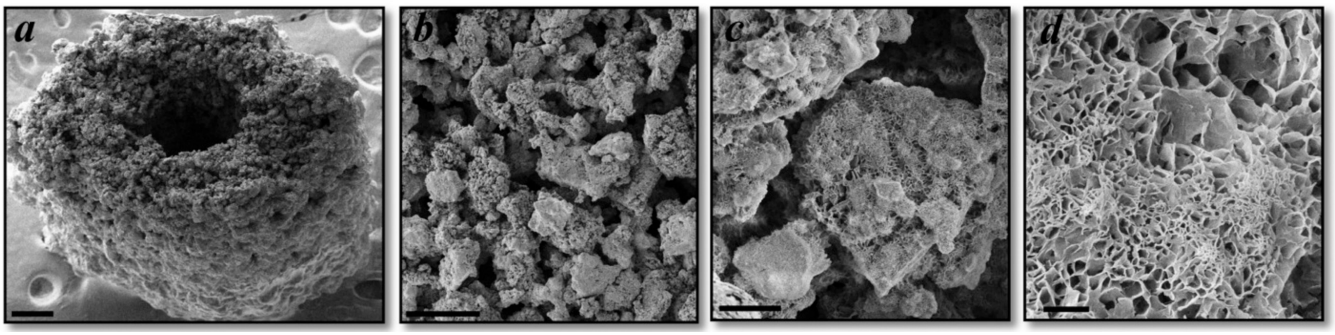


**Figure 3. Scanning electron micrographs demonstrating a 3D printed murine femoral scaffold with micro-porosity and plate-like crystal formation**

*a*) Murine-sized scaffold representing the geometry of the femoral mid-diaphysis for use in tissue engineering applications and preclinical bone regeneration studies. Scale bar is 250 μm. *b,c*) The 3D printing process produces scaffolds with intrinsic micro-porosity, primarily in the range of 20–50 μm, which is consistent with measurements from micro-CT images. Scale bars are 100 μm (*b*) and 10 μm (*c*). *d*) Plate-like crystal growth occurs on the surface of unreacted calcium phosphate particles, which increases the specific surface area for protein or drug adsorption. Scale bar is 1 μm.

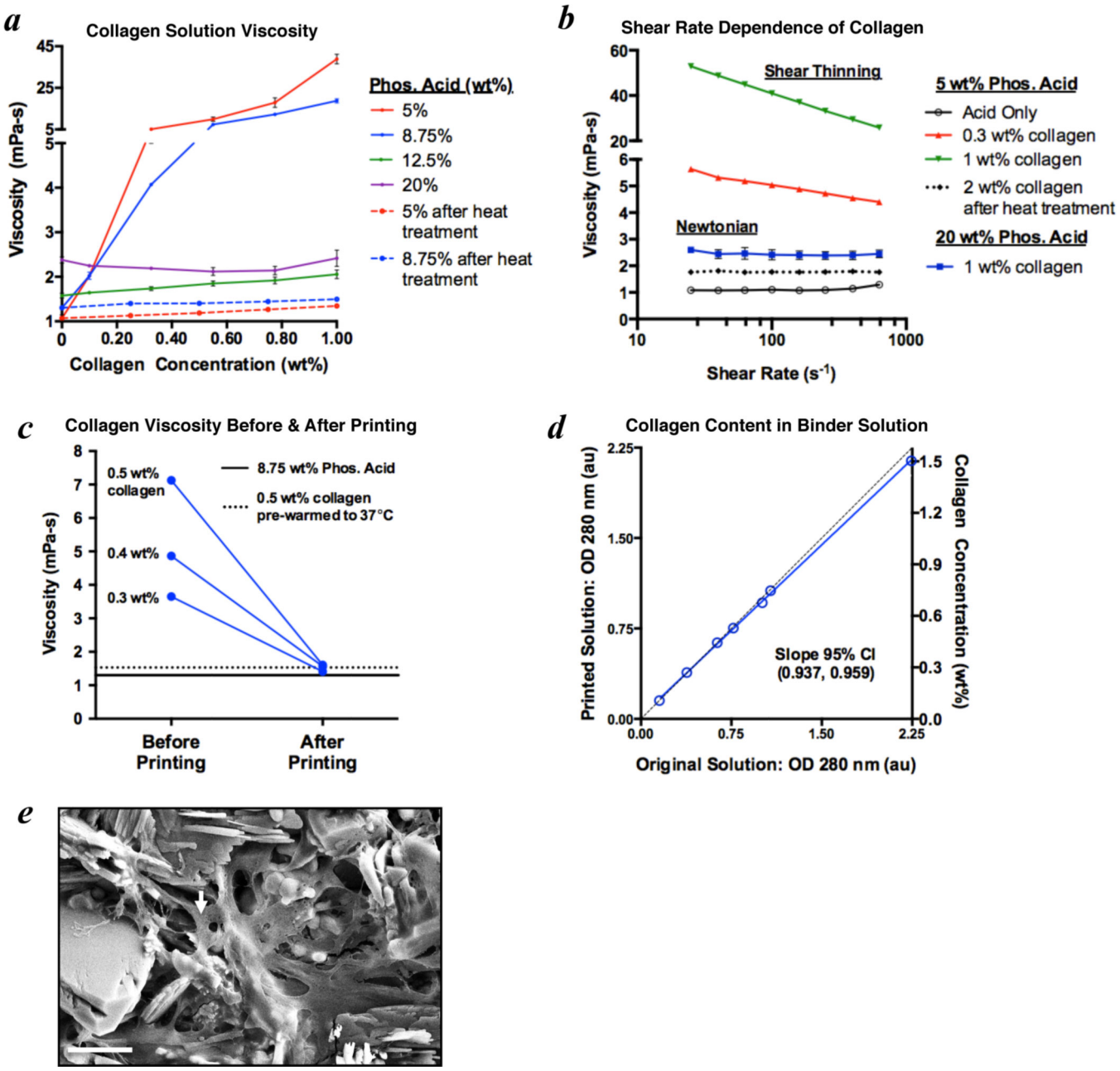


**Figure 4. Viscosity adjustment of collagen solutions in phosphoric acid enables 3D inkjet printing of collagen-calcium phosphate composites**

*a*) The viscosity of collagen in phosphoric acid solutions increases exponentially with collagen concentration at lower acidities (5 and 8.75 wt%), impeding inkjet printing. A brief heat treatment of collagen solutions at 37°C for 30 minutes dramatically reduces the viscosity (measured at 25°C) to ranges appropriate for inkjet printing. *b*) Interactions among collagen chains cause the exponential viscosity increase, as demonstrated by the shear thinning present with 0.3 wt% and 1 wt% collagen in 5 wt% phosphoric acid. With higher acid concentrations (≥12.5 wt%), or after heat treatment at 37°C for 30 minutes, the collagen is likely no longer in a fibrillar chain form. This denaturation results in Newtonian behavior

and minimal changes in viscosity with collagen concentration. *c*) The viscosity of collagen solutions in 8.75 wt% phosphoric acid decreases dramatically after printing from the inkjets, which likely results from chain denaturation associated with the thermal printing process. *d*) The printed solutions were confirmed to maintain at least 94% collagen content based on the optical density (OD) at 280 nm, indicating that reductions in collagen concentration do not explain the reduced viscosity. *e*) Scanning electron micrograph demonstrating collagen (arrow), delivered via the inkjets, dispersed among the bound calcium phosphate crystals in a 3D printed scaffold. Scale bar is 5 μm.

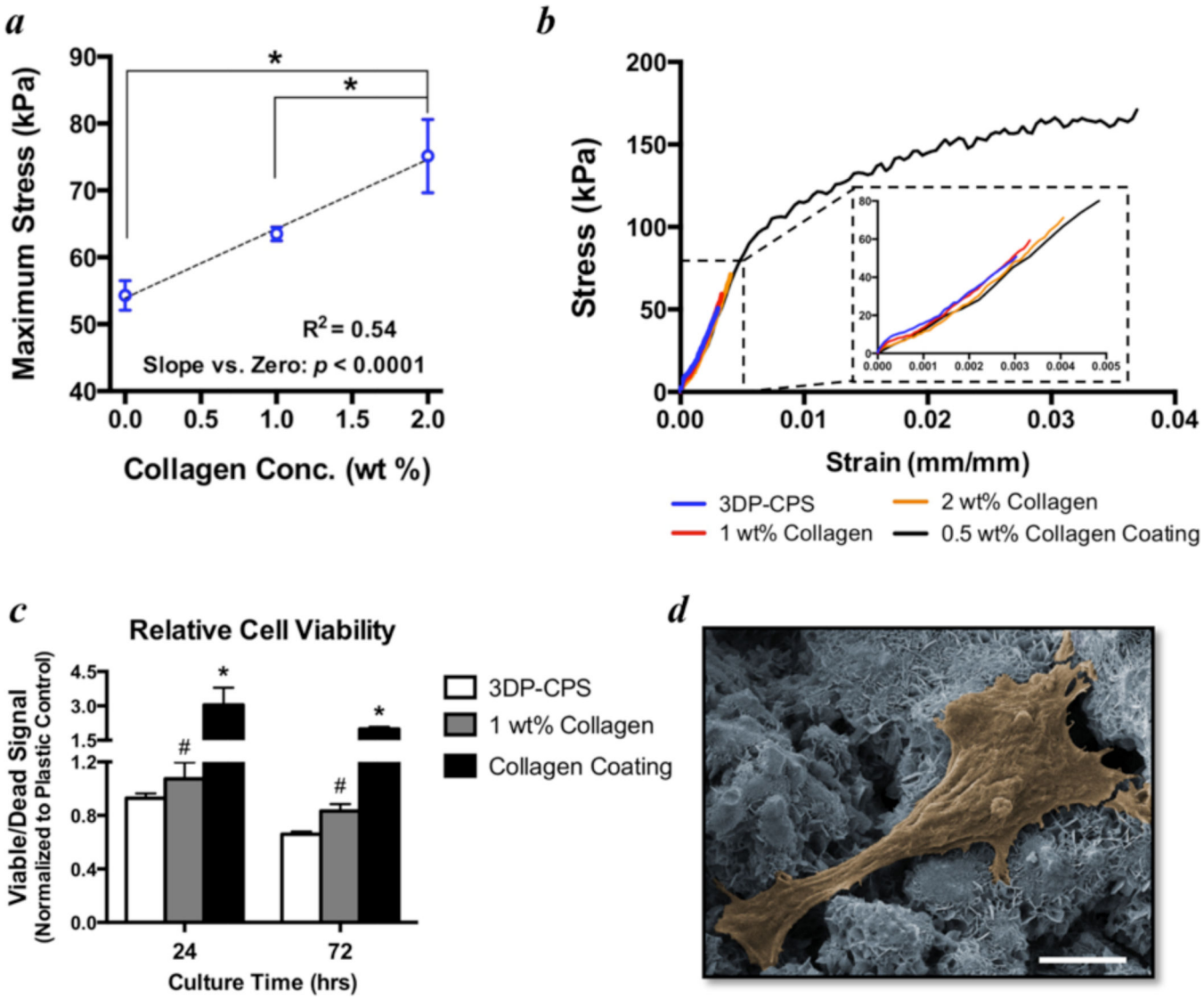


**Figure 5. Flexural strength and cell viability is significantly improved by collagen in the binder solution**

*a*) Maximum flexural strength is significantly increased with increasing concentrations of collagen in the binder solution (8.75 wt% phosphoric acid + 0.25 wt% Tween 80). Points represent means and error bars are standard error of the mean. n=8–9/group. * indicates $p < 0.05$ by ANOVA with Tukey's correction for multiple comparisons. Linear regression analysis confirms the slope is significantly different from zero with an $r^2 = 0.54$. *b*) Group-averaged 3 point flexure stress-strain curves demonstrate the increasing strength with collagen in the binder solution (1 and 2 wt%), but a persistent brittleness of these materials. Coating the baseline 3D printed calcium phosphate scaffold (3DP-CPS) materials with a 0.5 wt% neutralized fibrillar collagen film significantly improves the flexural strength and toughness. *c*) Adding 1 wt% collagen into the binder solution significantly improves the relative viability (normalized to tissue culture plastic) of C3H/10T1/2 cells cultured on 3D printed discs relative to controls without collagen (3DP-CPS). # indicates $p < 0.05$ by ANCOVA comparing 3DP-CPS to 1 wt% collagen binder with culture time as the covariate.

* indicates $p < 0.05$ compared to tissue culture plastic by ANOVA with Tukey's correction for multiple comparisons. n=5/group. Bars represent means and error bars represent standard error of the mean. *d*) Pseudo-colored SEM image of a representative cell on a collagen-calcium phosphate composite that was 3D printed with 1 wt% collagen in the binder solution. Of note is that the cell is attached to and spreading out on the material, which is indicative of a healthy cell. Scale bar is 5 μm.

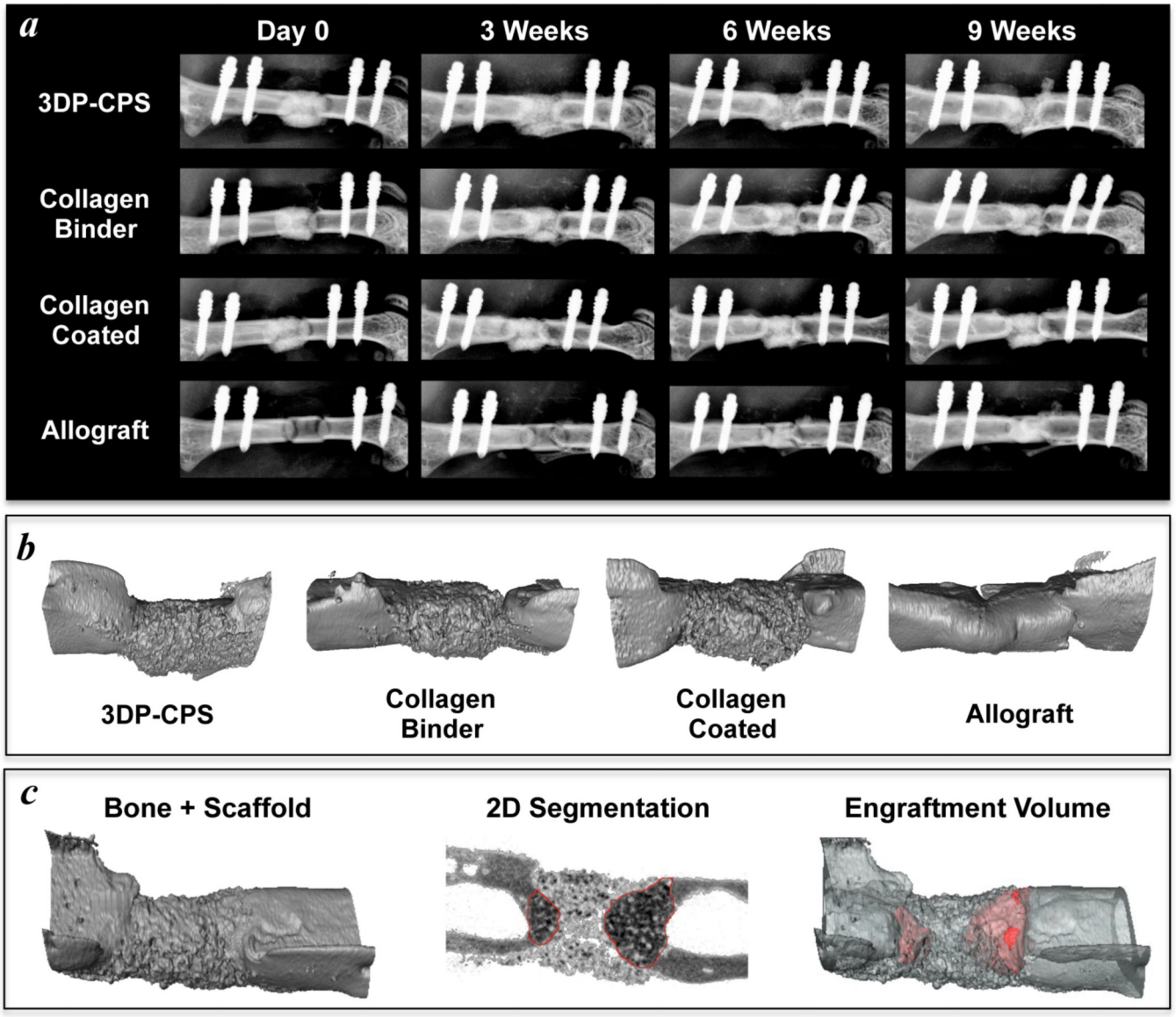


**Figure 6. 3D printed calcium phosphate scaffolds are osteoconductive and enable bone ingrowth in a critically sized murine femoral defect**

X-rays of the bone healing time course (*a*) and 3D micro-CT renderings at 9 weeks (*b*) demonstrate similar levels of new bone formation between allografts, 3D printed calcium phosphate scaffolds (3DP-CPS), and 3DP-CPSs with 1 wt% collagen supplementing the binder solution (Collagen Binder). 3DP-CPSs that were coated with a 0.5 wt% neutralized fibrillar collagen (Collagen Coated) tended to facilitate less new bone formation. *c)* The volume of newly formed bone that contained scaffold material (red; engraftment volume) was quantified through manual contouring coupled with automated edge detection in the 2D micro-CT slices.

**Table 1**

Fluid Characteristics of Phosphoric Acid-Based Binder Solutions

| Acidity (wt %) | Collagen (wt %) | Tween 80 (wt %) | Printing Saturation (L/P) | Surface Tension (mN/m) | Viscosity (mPa-s) | Density (g/mL) |
|---|---|---|---|---|---|---|
| **5** | **0** | **0** | 0.06 ± 0.01 | 68.0 ± 1.0 | 1.07 ± 0.08 | 1.04 ± 0.03 |
| **5** | **0** | **0.25** | 0.23 ± 0.03 | 42.1 ± 1.3 | 1.05 ± 0.02 | 1.06 ± 0.04 |
| **8.75** | **0** | **0** | 0.14 ± 0.01 | 68.9 ± 0.8 | 1.30 ± 0.04 | 1.08 ± 0.03 |
| **8.75** | **0** | **0.25** | 0.23 ± 0.02 | 46.5 ± 1.8 | 1.44 ± 0.08 | 1.09 ± 0.02 |
| **8.75** | **1**[#] | **0** | 0.07 ± 0.01[*] | 55.0 ± 2.1 | 1.50 ± 0.11 | 1.10 ± 0.04 |
| **8.75** | **1**[#] | **0.25** | 0.22 ± 0.03 | 44.6 ± 1.7 | 1.72 ± 0.04 | 1.10 ± 0.03 |
| **3D Systems zb®61 Binder** | | | 0.28 ± 0.02 | 33.2 ± 0.2 | 1.01 ± 0.03 | 1.02 ± 0.03 |

[#]Collagen solutions were warmed to 37°C for 30 min and allowed to return to 20–25°C before all measurements

[*]Printing collagen solutions without Tween 80 tends to be inconsistent, often with heterogeneous saturation and streaking. L/P is volumetric liquid to powder ratio.

**Table 2**

Summary of Micro-CT and Torsion Measurements

| | Maximum Torque (N.mm) | Net Mineralized Volume# ($mm^3$) | Mineral Density ($mg/cm^3$) | Mineral Content (mg) | Scaffold Engraftment (% volume) |
|---|---|---|---|---|---|
| **3DP-CPS (n=4)** | 0.74 ± 0.47 | 0.59 ± 0.20 | 1068 ± 33 | 4.56 ± 0.30 | 27.0 ± 6.0 |
| **Collagen Binder (n=3)** | 0.80 ± 0.27* | 0.47 ± 0.34 | 1112 ± 52 | 4.63 ± 0.55 | 29.7 ± 13.6 |
| **Collagen Coated (n=4)** | 0.48 ± 0.18 | 0.41 ± 0.11 | 1026 ± 24 | 4.18 ± 0.12 | 7.7 ± 5.8 |
| **Allograft (n=4)** | 7.5 ± 3.4* | 1.15 ± 0.31 | 1095 ± 21 | 2.80 ± 0.38 | – |
| **Empty (n=3)** | 0.08 ± 0.05 | 0.52 ± 0.30 | 1085 ± 10 | 0.57 ± 0.33 | – |

Values are represented as means and standard error of the mean

* indicates $p<0.05$ compared with Empty by Kruskal-Wallis non-parametric ANOVA with Dunn's correction for multiple comparisons

# Mineralized volume less the average baseline (pre-implantation) scaffold or allograft volume

3DP-CPS: 3D printed calcium phosphate scaffold